Yan *et al. Chin. J. Mech. Eng.* (2019) 32:31
https://doi.org/10.1186/s10033-019-0345-7

Chinese Journal of Mechanical Engineering

ORIGINAL ARTICLE Open Access

Analysis of the Internal Characteristics of a Deflector Jet Servo Valve

Hao Yan*, Yukai Ren, Lei Yao and Lijing Dong

Abstract

In current research on deflector jet servo valves, the receiver pressure estimated using traditional two-dimensional simulation and theoretical calculation is always lower than the experimental data; therefore, credible information about the flow field in the prestage part of the valve can hardly be obtained. To investigate this issue and understand the internal characteristics of the deflector jet valve, a realistic numerical model is constructed and a three-dimensional simulation carried out that displays a complex flow pattern in the deflector jet structure. Then six phases of the flow pattern are presented, and the defects of the two-dimensional simulation are revealed. Based on the simulation results, it is found that the jet in the deflector has a longer core area and the fluid near the shunt wedge cannot resist the impact of the high-speed fluid. Therefore, two assumptions about the flow distribution are presented by which to construct a more complete theoretical model. The receiver pressure and prestage pressure gain are significantly enhanced in the calculations. Finally, special experiments on the prestage of the servo valve are performed, and the pressure performance of the numerical simulation and the theoretical calculation agree well with the experimental data. Finally, the internal mechanism described by the theoretical and numerical models is verified. From this research, more accurate numerical and theoretical models are proposed by which to figure out the internal characteristics of the deflector jet valve.

Keywords: Deflector jet, Servo valve, Computational fluid dynamics (CFD), Numerical simulation

1 Introduction

An electro-hydraulic servo valve plays an important role in energy conversion and control of hydraulic equipment. However, this type of valve is characterized by strong coupling of fluid, complex structures, electromagnetic activity, and temperature distribution. Due to its complexity, researchers have been concentrating on a variety of servo valves for years [1, 2]. Compared with more traditional nozzle flapper or jet-pipe servo valves, a deflector jet servo valve (DJV) was designed with consideration of both pollution resistance and dynamic performance, and has become a new crucial focus of activity.

It is generally accepted that the research on DJVs is derived from the jet pipe valves. Somashekhar et al. [3] established a numerical model including a jet pipe valve's hydrostatic pressure cavities and armature components, and the effect of the fluid structure interaction on the equilibrium was analyzed. How the wall surface roughness acts on the jet flow pattern was analyzed by Pham [4]. Then other scholars built numerical models of the jet pipe valve [5, 6], and the effect of various factors on the jet characteristics was studied by RANS simulation [7, 8].

By comparison, the hydraulic amplifier of a DJV is more complex because of a V-shaped tapered slit in the deflector and the particular shape of the receiving port. Applying the standard k-ε turbulence model, Dhinesh [9] confirmed that the pressure difference of the two control chambers in the numerical simulation was lower than the experimental value, which was not explained. Then other scholars also carried out RANS simulations [10–12] and tried to explore the influence of the structural parameters, machining technologies, and external conditions on the flow pattern [13, 14]. In 2015, Yin et al. [15] built a simplified 3D model, using an RNG k-ε turbulence model to analyze the factors affecting cavitation. Then Jiang et al. [16] constructed a 3D model using tetrahedral meshes

*Correspondence: hyan@bjtu.edu.cn
School of Mechanical, Electronic and Control Engineering, Beijing Jiaotong University, Beijing 100044, China

and obtained more detailed simulation results. However, for these 3D models, the flow field was assumed to have a uniform thickness and the same outflow location as the 2D model, which is not quite consistent with the actual structure. In terms of theoretical exploration, Dhinesh [9] and other scholars [17–20] built flow and pressure analytical equations based on throttling theory, which were different from the phenomenon of simulation. Assuming that the jet was submerged and that the flow in the receiver was a piston, Li [5] made progress in the theoretical description of the receiver flow pattern. On the basis of the jet wall attachment theory, Yan et al. [21] modelled the flow distribution in the deflector analytically. Then Yan et al. [22, 23] applied the impact jet theory to the description of the DJV's two jets and proposed an integrated theoretical model. With regard to experimental research, Li [24] established a visualized DJV jet prototype.

To sum up, the method for theoretical exploration of the DJV is shifting from throttling theory to jet theory, and the 2D numerical model is being replaced by a 3D one. However, the experimental results hardly conform to theoretical calculations and simulations. Specifically, the receiver pressure from simulation and theoretical calculation is always lower than the experimental values. Therefore, for the prestage pressure gain, it is very difficult to obtain consistent results in calculations, simulations, and experiments. To solve these issues and attain a better description of the DJV internal flow characteristics, a 3D numerical model with consideration of the return flow along the force feedback rod was built. Meanwhile, two essential assumptions were presented for modification of the theoretical model. Finally, an experiment on the receiver pressure was performed to verify the above theoretical and simulated analyses.

2 Theoretical Description of DJV

2.1 DJV Prestage Jet Process

According to the deflector-jet-valve energy conversion mechanism, the flow process is divided into the four stages shown in Figure 1. Hydraulic oil is injected at the inlet under high pressure and reaches the deflector, which is referred to as the first jet. After contact of the oil with the deflector, a high-pressure zone is generated and this stage is called the deflector pressure recovery. Then the oil is ejected from the outlet of the deflector, known as the second jet. Finally, new high-pressure zones occur in the two receivers, which process is referred to as the receiver pressure recovery.

2.2 Velocity Distribution of the First Jet

The DJV parameters are defined in Figure 2, with values shown in Table 1. A previous study [22] shows that the jet procedure can be regarded as a free submerged turbulent

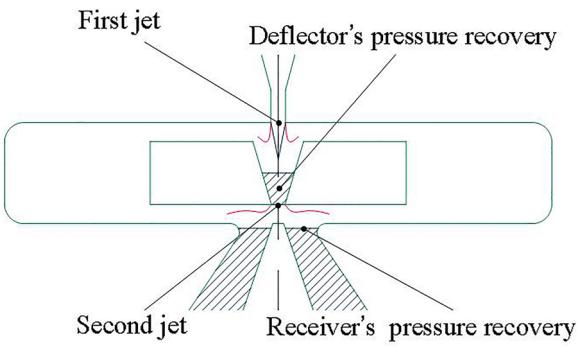

Figure 1 Four stages of the deflector jet process

jet, and that the fluid pressure energy is converted into kinetic energy. However, we think that the friction loss from reduction of the flow should be considered, so the average velocity of the first jet can be obtained as

$$\frac{p_0 - p_b}{\rho g} = (1 + \zeta_0)\frac{u_0^2}{2g}, \tag{1}$$

$$\zeta_0 = \frac{\lambda}{8\tan\alpha}\left[1 - \left(\frac{2b_0}{A_1}\right)^2\right], \tag{2}$$

where u_0 is the average velocity of first jet, ζ_0 is the local loss coefficient, and λ is the pipe's friction coefficient (which was set to 0.62 empirically). Then, according to Eqs. (1) and (2), the first jet's average velocity can be computed with the result that $u_0 = 178.2$ m/s.

Moreover, it was discovered that the fluid is affected by the friction of the jet channel wall, so the velocity distribution at the inlet is not uniform. The 2D numerical simulation shows that the velocity distribution is approximately trapezoidal. Therefore, we define a fitting trapezoid with the average velocity u_0 to describe the inlet velocity, as illustrated in Figure 3.

In the simulation result, the velocity of the fluid rises with increase of its distance from the inner wall at the rate of 2.25 (m/s)/μm. To ensure that the average velocity is equal to the calculated value u_0, it is convenient to learn that the initial width of the core area $2b_1 = 0.12$ mm and that the velocity in the core area $u_1 = 195$ m/s. Therefore, different from traditional opinion, the initial width of the core area is less than the jet's width.

In addition, according to the 2D simulation, the jet core area is terminated early because of the joint effect of the jet's trapezoidal velocity distribution and the sidewalls of the deflector's V-shaped structure. These cause the jet to reach the primary phase prematurely. Therefore, we suppose that the reducing angle of the core area is approximately equal to the inclination angle of the sidewall, as

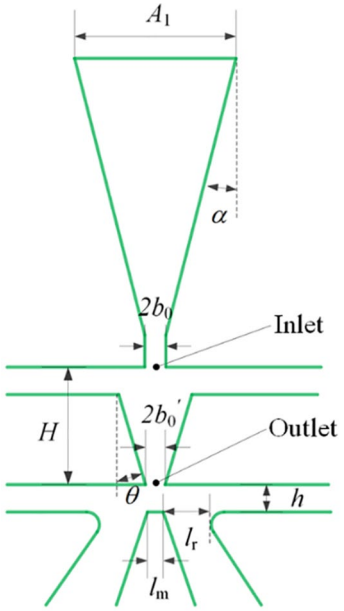

Figure 2 Definition of parameter

Table 1 Values of the DJV parameters

Parameter	Value
First jet half-width b_0 (m)	7.498×10^{-5}
Second jet half-width b'_0 (m)	7.012×10^{-5}
Inflow width A_1 (m)	1.147×10^{-3}
Shunt wedge width l_m (m)	1.09×10^{-4}
Receiver width l_r (m)	1.9×10^{-4}
Inflow angle α (°)	13
Sidewall's inclination angle θ (°)	16.5
Hydraulic oil density ρ (kg/m^3)	847
Initial pressure P_0 (MPa)	21
Jet back pressure P_b (MPa)	3.1
Gravity acceleration g (m/s^2)	9.8
Deflector's distance H (m)	8.84×10^{-4}
Second jet height h (m)	1.95×10^{-4}

shown in Figure 4. As a result, the length of the core area can be expressed as

$$L_0 = \frac{b_0}{\tan\theta} = 3.388 b_0. \tag{3}$$

In the primary phase, the turbulent jet appears similar to that in Forthmann's experimental data [25]. Then supposing that u_m is the velocity on the axis, the location where the flow velocity $u = u_m/e$ is regarded as the jet's boundary. This is described by the Eigen half width b_e, as shown in Figure 4. In the primary phase, the velocity distribution in the orthogonal direction of the jet's axis approximately accords with a Gaussian distribution [26]. That is,

$$\frac{u}{u_m} = \exp\left(-\frac{y^2}{b_e^2}\right), \tag{4}$$

where u is the velocity at the coordinate y.

Assuming that the jet's width is linearly extended, the expansion coefficient ε can be introduced. Then,

$$b_e = \varepsilon x. \tag{5}$$

According to Eqs. (4) and (5), the velocity distribution at any section in the primary phase can be expressed as

$$u = u_m \exp\left[-\frac{y^2}{(\varepsilon x)^2}\right]. \tag{6}$$

Moreover, for a certain section, the momentum flux per unit thickness, abbreviated as the momentum, can be calculated as

$$M = \int_{-\infty}^{+\infty} \rho u^2 \mathrm{d}y. \tag{7}$$

Then we can compute the initial momentum of the first jet as follows:

$$M_0 = 2\int_0^{b_0} \rho u^2 \mathrm{d}y = 1.56 \rho u_1^2 b_0, \tag{8}$$

and from Eqs. (6) and (7), the momentum at an arbitrary section is

$$M = 2\rho \int_0^{+\infty} u_m^2 \exp^2\left(-\frac{y^2}{b_\varepsilon^2}\right)\mathrm{d}y = \rho\sqrt{\frac{\pi}{2}} u_m^2 \varepsilon x. \tag{9}$$

Because of conservation of momentum, the momentum at the arbitrary section in the primary phase is equal to the initial momentum (i.e., $M = M_0$). Thus, from Eqs. (8) and (9) we can acquire the equation

$$\frac{u_m}{u_1} = \left(\sqrt{\frac{2}{\pi}}\frac{1}{\varepsilon}\right)^{\frac{1}{2}} \left(\frac{26 b_0}{15x}\right)^{\frac{1}{2}}. \tag{10}$$

Supposing that $\varepsilon = 0.348$ according to Alberson's experiments [27], Eq. (10) can be simplified as

$$u_m = 1.51\left(\frac{26 b_0}{15x}\right)^{\frac{1}{2}} u_1. \tag{11}$$

Furthermore, substituting Eq. (11) into Eq. (6), the velocity distribution of the primary phase can be represented as

$$u = 0.55\left(\frac{1}{x}\right)^{\frac{1}{2}} u_1 \exp\left[-\left(\frac{y}{0.348x}\right)^2\right]. \tag{12}$$

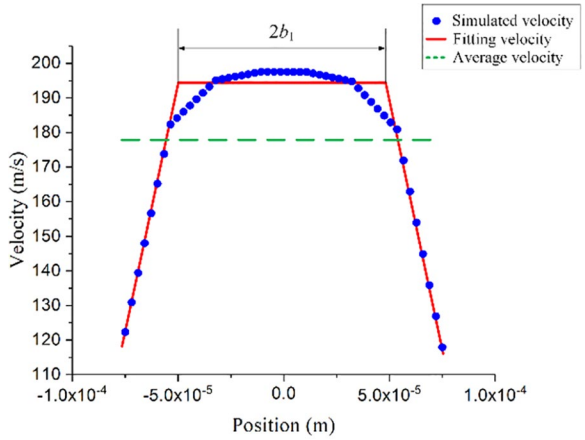

Figure 3 First jet's velocity distribution at the inlet

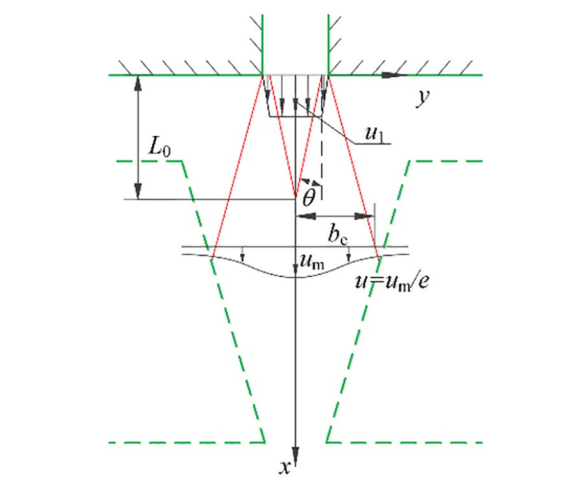

Figure 4 Description of the jet structure

2.3 Stagnation Point in the Deflector

According to previous research [22], there exists a stagnation point M_r on the sidewall, as shown in Figure 5. Then the fluid below the stagnation point flows downstream along the sidewall and the fluid above flows upstream to the low-pressure zone and returns to the tank. In such cases, y_r represents the distance from the stagnation point to the jet axis and y_0 is the distance from the jet's boundary at section $M_r's$ to the jet axis.

According to the wall attachment jet model of Bourque [28] and supposing conservation of momentum, the total momentum along the sidewall is

$$J_0\cos(\theta) = J_1 - J_2, \tag{13}$$

where J_1 is the momentum entering the high-pressure zone along the sidewall, J_2 is the return momentum along the sidewall, and J_0 is the initial momentum along the jet axis. Moreover, according to the velocity distribution, these momentums can be calculated as

$$J_1 = \int_0^{y_r} \rho u^2 \mathrm{d}y, \tag{14}$$

$$J_2 = \int_{y_r}^{y_0} \rho u^2 \mathrm{d}y, \tag{15}$$

and

$$J_0 = \frac{1}{2} M_0. \tag{16}$$

Supposing that x_r is the distance between the stagnation point and the inlet section, y_r and y_0 can be computed by

$$y_r = (H - x_r) \cdot \tan(\theta) + b_0' + x_f, \tag{17}$$

and

$$y_0 = x_r \cdot \tan(\alpha) + b_0 + x_f, \tag{18}$$

where x_f is the deflector displacement. Then, according to Eqs. (13)–(18), we can obtain the stagnation point's location with the result that $x_r = 0.57$ mm, when x_f is zero.

Because of the sidewall's extrusion, the downstream fluid's kinetic energy is converted to pressure energy and a high-pressure area is generated, as illustrated in Figure 6. Similarly, we think that the energy loss of the reducing flow should be considered. Assuming that the deflector outlet's velocity is uniform and denoted by u_0', the energy conservation can be written as

$$\frac{1}{2}\rho \cdot 2b_0' {u_0'}^3 = \frac{1}{2} \cdot 2 \cdot \int_0^{y_r} (\rho u^3 - \zeta_1 \rho u^3) \mathrm{d}y, \tag{19}$$

and

$$\zeta_1 = \frac{\lambda}{8\tan\theta}\left[1 - \left(\frac{b_0'}{y_r}\right)^2\right], \tag{20}$$

where ζ_1 is local loss coefficient. According to Eqs. (19) and (20), the second jet's velocity is attained, with the result that $u_0' = 152.5$ m/s.

2.4 Stagnation Point in the Deflector

The kinetic energy and the momentum at the outlet can be calculated as

$$E_0' = \rho b_0 {u_0'}^3, \tag{21}$$

and

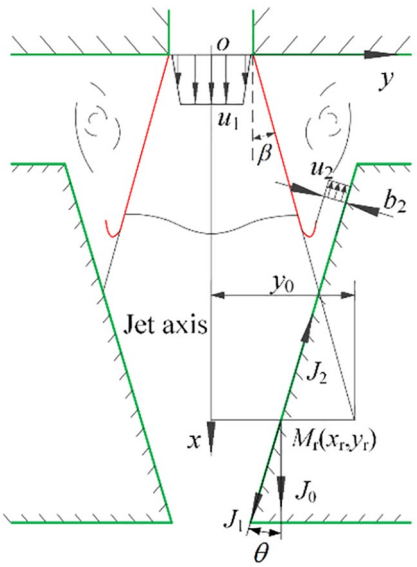

Figure 5 First jet's impact and stagnation point

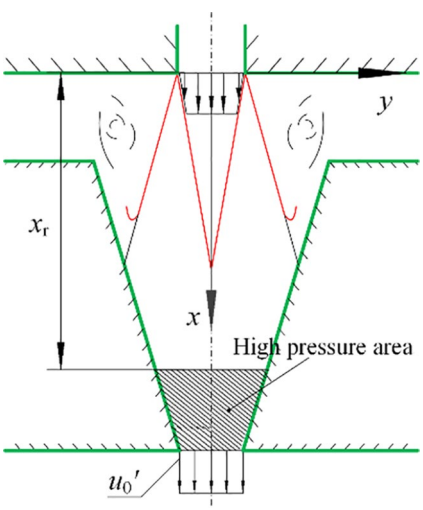

Figure 6 Deflector pressure recovery

$$M' = 2\rho b_0' u_0'^2. \tag{22}$$

Supposing that the fluid is incompressible, the jet will directly act on the receiver's oil surface and the shunt wedge, similar to an impact jet, as illustrated in Figure 7.

According to the turbulent impact jet's pressure distribution law, the pressure at a certain point on the impact surface can be written as

$$\frac{p}{p_s} = \exp\left[-\left(\lambda\frac{y}{b_p}\right)^2\right], \tag{23}$$

where p_s is the stagnation point's pressure on the impact surface, b_p is the distribution pressure's Eigen half width, and λ is the distribution coefficient.

Based on the impact jet theory, p_s can be described as

$$\frac{p_s}{\rho\frac{u_0'^2}{2}} \cdot \frac{h}{2b_0'} = const, \tag{24}$$

and empirically, the constant can be set to 2.135, so the stagnation pressure $p_s = 15.1$ MPa. Meanwhile, referring to the simulation results, we can determine that $b_p = 0.05$ mm and $\lambda = 0.833$. Then the pressure distribution on the impact surface can be computed using Eq. (23).

Therefore, on the impact surface, the pressure should follow the Gauss distribution. However, based on simulation results, we find that this conclusion is only applicable to the solid part of the impact surface. For the fluid surface, the pressure is approximately uniform and equal to the receiver's pressure. Thus, the momentum equation in the direction of the second jet axis can be written as

$$2\rho b_0' u_0'^2 = \int_{-\frac{l_m}{2}}^{\frac{l_m}{2}} p\mathrm{d}y + p_1 l_r + p_2 l_r, \tag{25}$$

where p_1 and p_2 are the two receivers' pressures, and l_r is the fluid part's width on the impact surface, as expressed in Figure 7.

Referring to Eq. (25) and assuming that the impact surfaces on both sides of the stagnation point have approximately equal effect on the momentum, the pressures in the two receivers can be calculated respectively as follows:

$$\begin{cases} p_1 = \frac{1}{l_r - x_f}\left\{\rho b_0' u_0'^2 - \int_0^{\frac{l_m}{2}-x_f} p_s \exp\left[-\left(\lambda\frac{y}{b_p}\right)^2\right]\mathrm{d}y\right\}, \\ p_2 = \frac{1}{l_r + x_f}\left\{\rho b_0' u_0'^2 - \int_0^{\frac{l_m}{2}+x_f} p_s \exp\left[-\left(\lambda\frac{y}{b_p}\right)^2\right]\mathrm{d}y\right\}, \end{cases} \tag{26}$$

where x_f is the deflector displacement, and it is positive when the deflector moves to the right. The receiver pressures for different deflector displacements are listed in Table 2.

The pressure gain of the prestage hydraulic amplifier can be computed by

$$K_p = \frac{p_1 - p_2}{x_f}. \tag{27}$$

If the deflector has no offset, the two receivers have the same pressure, which is referred to as the balance

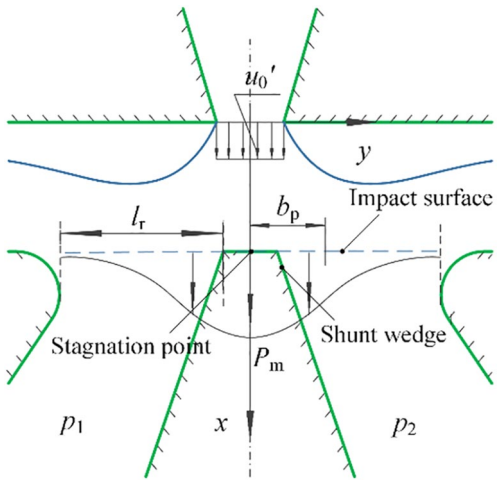

Figure 7 Second jet pattern

Table 2 Receiver pressures for different deflector displacements

Displacement (mm)	Left receiver (MPa)	Right receiver (MPa)
0.04	2.8	8.6
0.03	3.0	7.0
0.02	3.3	5.8
0.01	3.7	4.9
0	4.2	4.2
− 0.01	4.9	3.7
− 0.02	5.8	3.3
− 0.03	7.0	3.0
− 0.04	8.6	2.8

pressure p_r, which will be an important parameter for evaluating the accuracy of the theoretical model. According to Eq. (26), we learn that $p_r = 4.2$ MPa.

Unfortunately, it is noticed that the balance pressure p_r is always much lower than the experimental data, which is a problem that has plagued researchers for a long time. Moreover, the prestage pressure gain is calculated based on the receiver pressure, so a large error is caused.

3 Three-dimensional Numerical Simulation

3.1 Flow Distribution of the 3D Simulation

Because the structure of the deflector valve is very small and complex, in order to explore the internal flow pattern, explain the inaccuracy of the theoretical model, and modify the theoretical model, the numerical simulation needs to show the detailed features of the flow field intuitively.

To address the inaccuracy of the 2D simulation, a 3D model of the prestage fluid was constructed, as illustrated in Figure 8. Numerical simulations show that the mesh generation of the DJV's 3D model is very important. Any tiny unhealthy mesh might cause the simulation's divergence or the result's significant incorrectness. Because the deflector jet structure is quite sophisticated and the complexity level of each part is significantly different, the geometric model needs to be partitioned before mesh generation. For the critical parts of the flow field, such as the jet inlet, the deflector's V-shaped structure, and the receiver entrances, denser hexahedral meshes were applied, as shown in Figure 9.

However, in the parts, such as the inflow chamber and the receiver chambers, the fluid's momentum does not change dramatically, so the tetrahedral meshes were adopted and their size made consistent with the local scale of the flow field, as shown in Figures 10 and 11.

Therefore, without affecting the simulation accuracy, the difficulty of mesh generation and the requirement for computer capacity were reduced. Although automatic mesh generation technology was implemented, some low quality meshes needed to be dealt with. Finally, the deflector jet structure's 3D model with 5441561 meshes was obtained, as shown in Figure 12.

Based on the standard k-ε turbulent model, the 3D flow field was simulated and it was ensured that all the residuals were less than 10^{-5}. Boundary conditions are shown in Table 3, and the simulation parameters are given below. The hydraulic diameters of the inlet and the outlet are 1.15 mm and 1.03 mm, and the turbulence intensity is 10%. In order to improve the precision of calculation, the second-order upwind was selected in the simulation. Figure 13 displays the velocity vectors of the flow field and clearly describes the flow pattern of the first jet, the second jet, and the impact jet near the receivers.

In order to observe the pressure distribution of the flow field, the pressure contour of typical sections was extracted, as shown in Figure 14. It was learned that the pressure in the flow field was approximately equal to the back pressure, except in the inlet chamber, V-shaped structure, and the receiver chambers.

Figure 15 shows the central section's pressure contour. According to the 3D simulation, the negative pressure area is too small to display and is attached to both sides of the shunt wedge; thus, almost all the regions have positive pressure. That is, there will be no cavitation on both sides of the second jet. The receiver pressures reach 5.3 MPa, which is much higher than the theoretical calculation and 2D simulation. However, this result matches the experiment better. The balance pressures obtained by different methods are listed in Table 4.

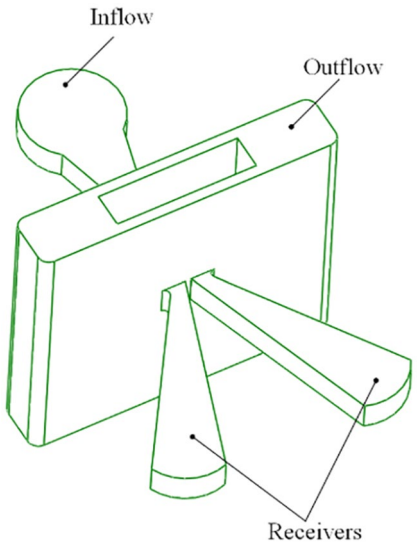

Figure 8 Deflector jet structure's 3D model

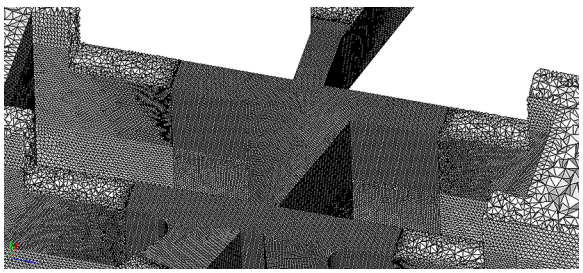

Figure 9 Critical parts mesh generation

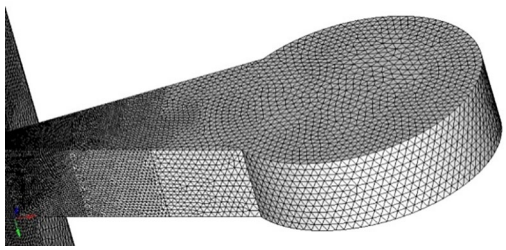

Figure 10 Inflow chamber's tetrahedral meshes

Therefore, compared with 2D numerical simulation and previous calculations, the new 3D numerical model has a more accurate result for the balance pressure, which can prove the validity of this numerical model to a certain extent.

With regard to the velocity distribution, the simulation shows that there is no obvious reflux in the V-shaped structure, which means little energy loss. Remarkably, the core area of the first jet is significantly longer and almost penetrates the deflector, as shown in Figure 16. All these results are quite different from the theoretical analysis and 2D simulation.

Moreover, the pressure along the impact surface in the 3D simulation is higher than that in the 2D simulation, as shown in Figure 17. It is worth noting that the 3D simulated pressure-drops on both sides of the shunt wedge are much greater than in the 2D simulation and two pressure singularities occur, which should be related to the higher velocity of the second jet. This discovery shows that the fluid close to the shunt wedge cannot resist the impact of the second jet. The problem now with the 3D jet is the existence of microscale cavitation caused by the pressure singularities.

3.2 Discussion on the Flow Pattern

Obviously, the 3D model is more consistent with the actual structure, so a new opportunity is provided to estimate the flow pattern in the deflector jet structure. First, a streamline graph was obtained, as shown in Figure 18, which shows that the flow in the deflector jet structure is never a planar flow as assumed in the 2D simulation and in the theoretical model. Moreover, it contains a complicated flow pattern, including lots of vertical flow.

Observing the streamlines in the V-shaped structure, as shown in Figure 19, we can notice that there are two symmetrical vortexes in the deflector, and that vertical spiral flow exists. This spiral flow is representative and can be thought to be one of the important features of the deflector jet valve.

The complete flow path can be analyzed with reference to Figure 20. After the fluid enters the deflector at the inlet, it passes through the deflector and the gaps on both sides of the deflector many times, and finally returns to the outflow interface with the back pressure. The complexity of this flow is far beyond the description in the 2D simulation.

Therefore, the flow in the deflector jet structure can be divided into the six phases shown in Figure 20. Phase 1 is the forward flow, which starts from the inlet and passes through the deflector. Phase 2 is the return flow after impacting the deflector, which means that the oil returns to back pressure zones on both sides after the second jet. Phase 3 is defined as entrainment flow. The first jet leads to the entrainment effect, causing the oil in the back pressure zone to flow to the inlet through the gap. Phase 4 is the spiral flow, by which the oil in the deflector finishes the spatial movement perpendicular to the central section. Phase 5 is the free flow in the back pressure zone, which has a random trajectory. Last, Phase 6 is departing flow, by which the oil leaves the structure and returns to the outflow interface. These six phases can be used to

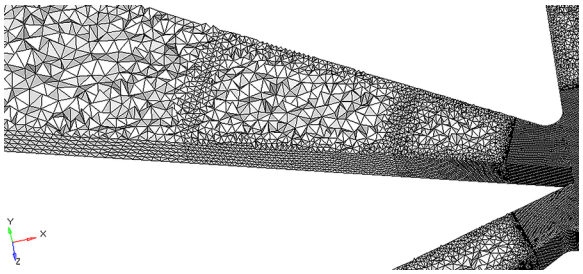

Figure 11 Receiver chamber's tetrahedral meshes

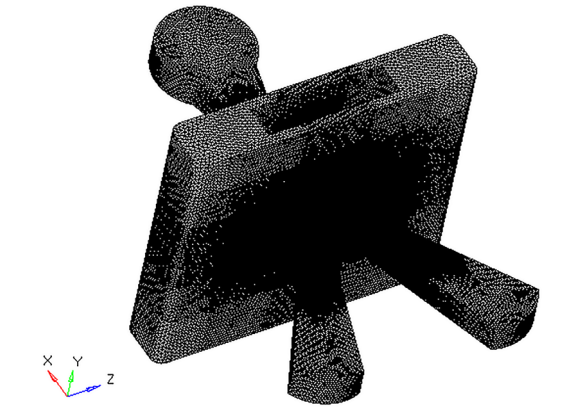

Figure 12 Mesh generation of whole model

Table 3 Boundary conditions

Parameter	Value
Oil density (kg/m^3)	849
Viscosity (kg/(m·s))	0.01026
Inlet pressure (MPa)	21
Outlet pressure (MPa)	3.1

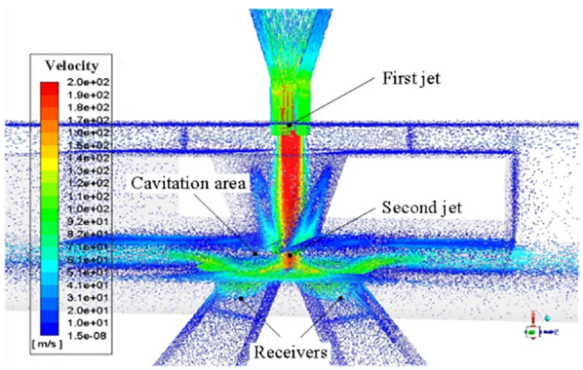

Figure 13 Velocity vectors of 3D flow

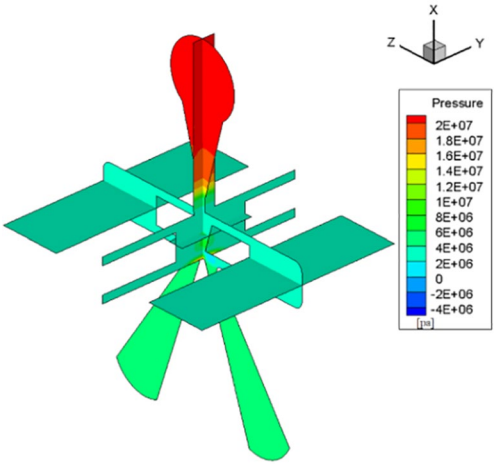

Figure 14 Pressure contour of typical sections

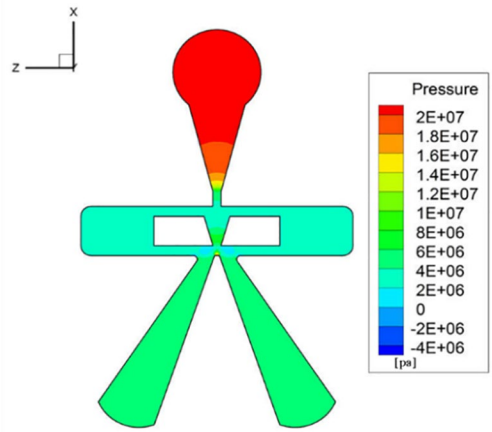

Figure 15 Pressure contour of the central section

Table 4 Comparison of the balance pressures

Parameter (MPa)	Value
Experimental result	5.6
Theoretical calculation	4.2
2D simulation calculation	4.8
3D simulation calculation	5.3

accurately describe the flow pattern in the deflector valve. However, with 2D simulation, only Phases 1 and 2 can be simulated properly. Remarkably, with regard to Phase 3, the 2D simulation shows the opposite flow direction. Therefore, the 3D simulation has much better credibility and the 2D simulation defects are identified.

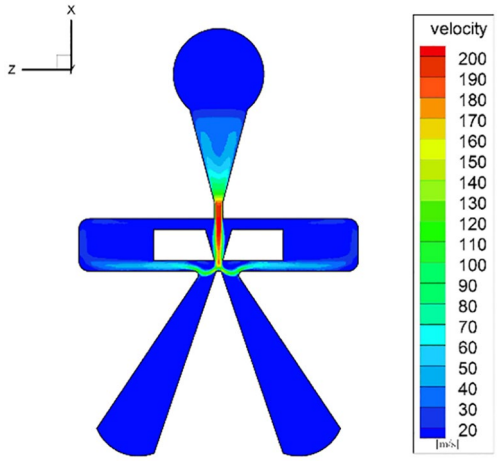

Figure 16 Velocity contour of the central section

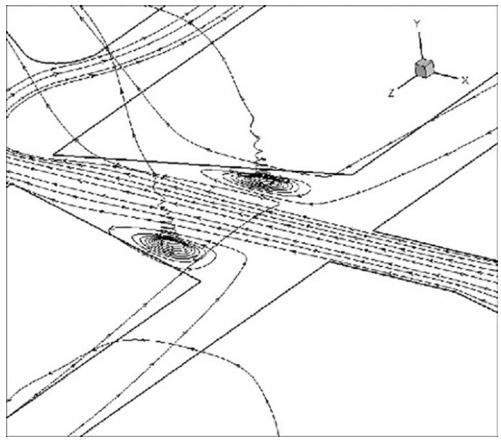

Figure 19 Spiral flow in the deflector

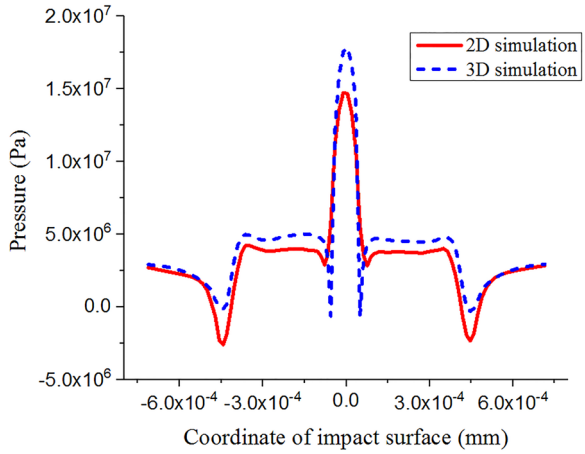

Figure 17 Pressure distribution along the impact surface

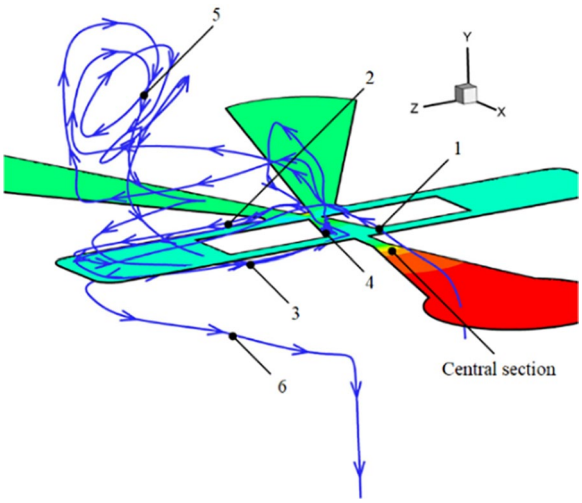

Figure 20 Analysis of the flow path

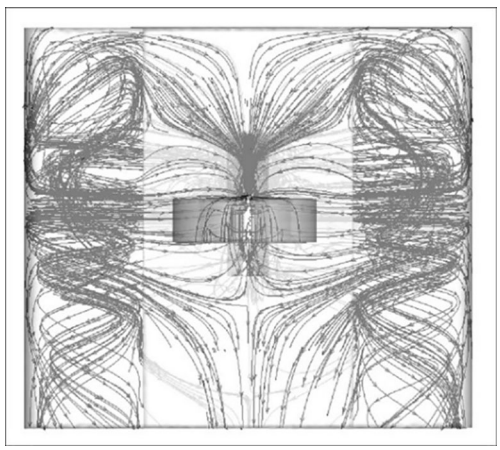

Figure 18 Streamlines in the deflector jet structure

4 New Assumptions and Modification of the Theoretical Model

4.1 Assumption of the Jet Core Length

According to the 3D simulation results, it was learned that the jet core is longer than in the previous theoretical assumption. To describe it more precisely, a new modified assumption is presented. That is, the first jet will terminate at the deflector outlet, as illustrated in Figure 21. Based on this assumption, the length of the core area L_0 is extended to 0.88 mm.

Meanwhile, it is still assumed that the velocity outside the core area accords with a Gaussian distribution. Thus, Eq. (5) can be modified as

$$b_e = \left(\varepsilon - \frac{b_1}{L_0}\right)x + b_1. \tag{28}$$

Substituting Eq. (28) into Eq. (4), the velocity distribution outside the core area can be expressed as

$$u = u_m \exp\left[-\frac{y^2}{\left(\left(\varepsilon - \frac{b_1}{L_0}\right)x + b_1\right)^2}\right]. \tag{29}$$

Because the core area terminates at the deflector's outlet, the expression of the momentum J_1 is rewritten as

$$J_1 = \int_0^{y_1} \rho u_1^2 \mathrm{d}y + \int_{y_1}^{y_r} \rho u^2 \mathrm{d}y, \tag{30}$$

where y_1 is the half width of the core area at the stagnation point.

Similarly, by solving Eq. (13) the stagnation point's location can be determined. The new calculation result is that $x_r = 0.624$ mm, which shows that the stagnation point has a downward shift after the modification. In the meantime, Eq. (19) is modified as

$$\frac{1}{2}\rho \cdot 2b_0' {u_0'}^3 = \frac{1}{2} \cdot 2 \cdot (1-\zeta_1)\left(\int_0^{y_1} \rho_1^3 \mathrm{d}y + \int_{y_1}^{y_r} \rho u^3 \mathrm{d}y\right). \tag{31}$$

Then the modified deflector outlet velocity can be computed again, with the result that $u_0' = 164.9$ m/s. Thus, the second jet's velocity increases after the modification.

4.2 Assumption of Receivers Effective Working Length

As mentioned above, the fluid close to the shunt wedge cannot resist the impact of the second jet; so the effective working length l_s is proposed, as shown in Figure 22.

When the deflector is in the central position, l_s can be computed as

$$l_s = l_r - \left(b_0' - \frac{l_m}{2}\right). \tag{32}$$

Consequently, replacing l_r with l_s, Eq. (26) can be rewritten as

$$\begin{cases} p_1 = \frac{1}{l_s - x_f}\left\{\rho b_0' {u_0'}^2 - \int_0^{\frac{l_m}{2} - x_f} p_s \exp\left[-\left(\lambda \frac{y}{b_p}\right)^2\right] \mathrm{d}y\right\}, \\ p_2 = \frac{1}{l_s + x_f}\left\{\rho b_0' {u_0'}^2 - \int_0^{\frac{l_m}{2} + x_f} p_s \exp\left[-\left(\lambda \frac{y}{b_p}\right)^2\right] \mathrm{d}y\right\}. \end{cases} \tag{33}$$

4.3 Calculation after Modification

Based on these new assumptions, a new calculation was performed, and the two receiver pressures with the new deflector displacements are shown in Table 5.

We learned that the updated receivers balance pressure p_r rises to 5.5 MPa, which is very close to the value in the 3D simulation, and the modification effect is illustrated in Figure 23. This shows that the receiver pressure after modification is remarkably increased as a whole, which is more consistent with the experimental result. However, the pressure variation tendency is similar to that before modification.

5 Experiment and Comparative Analysis

Although most of the internal physical quantities of the deflector jet structure are difficult to measure, an experiment on the receivers pressure characteristics was designed to verify the theoretical models and simulation results. The experimental device is shown in Figure 24.

An electric actuator was used to push one side of the torque motor's armature to drive the deflector, and the other side's tiny movement was measured simultaneously by a laser sensor. According to the parameters of the deflector jet structure, the displacement of the deflector can be calculated. In this way, the receiver pressures were detected, as shown in Table 6.

The experimental results show that when the deflector is in the central position, the pressure of the receiver is 5.6 MPa, which is closer to the theoretical calculation result (5.5 MPa) and the 3D simulation result (5.3 MPa). Thus, it can be deduced that this 3D numerical simulation is credible and that the new assumptions based on the 3D simulation are reasonable.

By comparing the theoretical calculation with the experimental data, it was learned that the modified theoretical model matches the experimental data well, especially when the deflector works near zero position, as illustrated in Figure 25. Moreover, Figure 26 describes two receivers' pressure difference characteristics. In fact, it seems that the modification of the theoretical model has little effect on the pressure difference characteristics, but the modified model greatly improves the computational accuracy of the pressure gain, as shown in Figure 27. Accordingly, the modification is of great significance for modeling the servo valve.

The experimental results show that when the deflector is in the central position, the pressure of the receiver is 5.6 MPa, which is closer to the theoretical calculation result (5.5 MPa) and the 3D simulation result (5.3 MPa). Thus, it can be deduced that this 3D numerical simulation is credible and that the new assumptions based on the 3D simulation are reasonable.

By comparing the theoretical calculation with the experimental data, it was learned that the modified theoretical model matches the experimental data well, especially when the deflector works near zero position, as illustrated in Figure 25. Moreover, Figure 26 describes

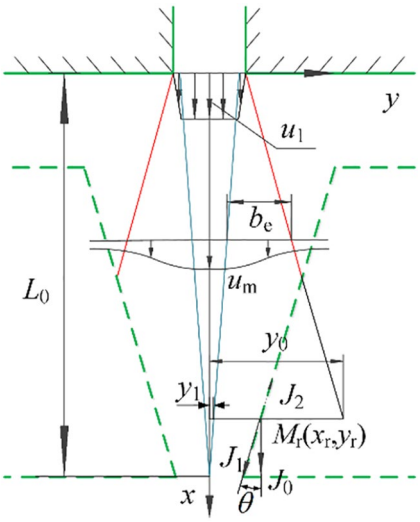

Figure 21 Longer core area assumption

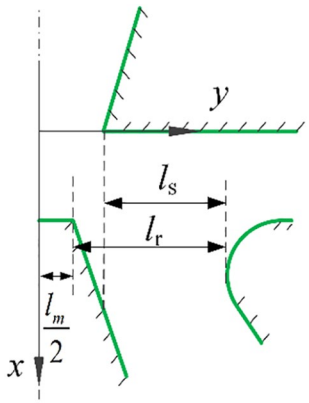

Figure 22 Effective working length of the receiver

Table 5 Receiver pressures after modification

Displacement (mm)	Left receiver (MPa)	Right receiver (MPa)
0.04	3.9	10.3
0.03	4.1	8.7
0.02	4.5	7.3
0.01	4.9	6.3
0	5.5	5.5
− 0.01	6.3	4.9
− 0.02	7.3	4.5
− 0.03	8.7	4.1
− 0.04	10.3	3.9

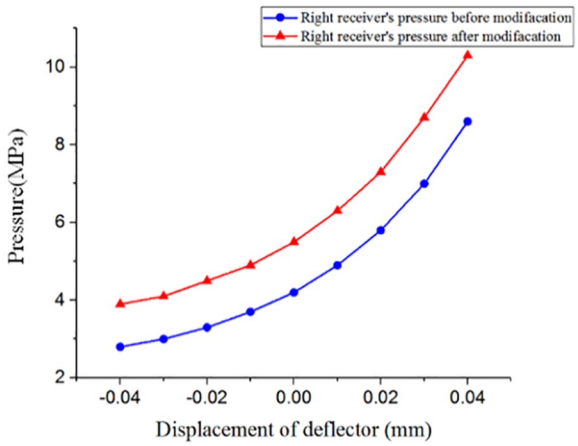

Figure 23 Effect of modification on the receiver pressure calculation

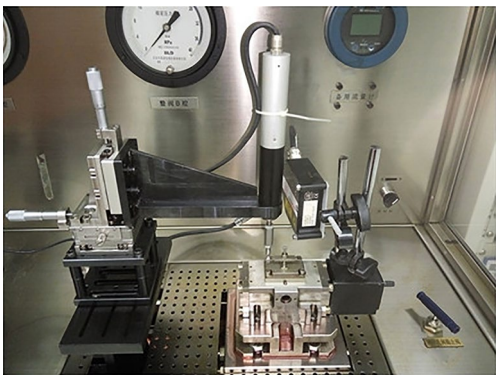

Figure 24 Experimental device

Table 6 Experimental results

Displacement (mm)	Left receiver (MPa)	Right receiver (MPa)
0.04	3.5	9.8
0.03	3.8	8.5
0.02	4.2	7.0
0.01	5.0	6.4
0	5.6	5.6
− 0.01	6.4	5.1
− 0.02	7.0	4.3
− 0.03	8.5	3.9
− 0.04	9.8	3.4

two receivers' pressure difference characteristics. In fact, it seems that the modification of the theoretical model has little effect on the pressure difference characteristics, but the modified model greatly improves the computational accuracy of the pressure gain, as shown in

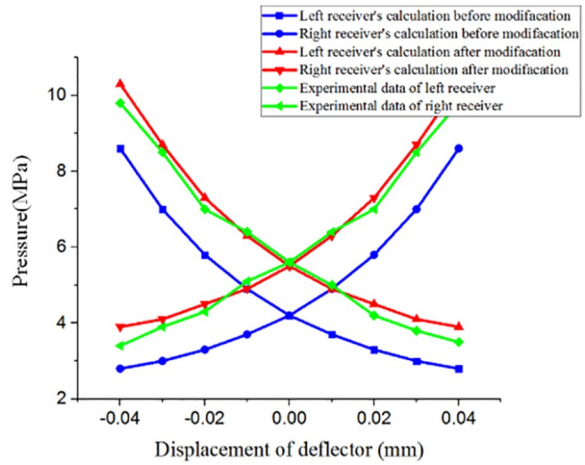

Figure 25 Comparison of the pressure characteristics

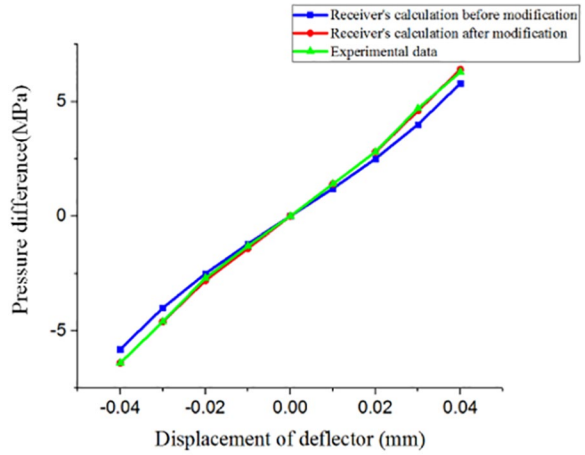

Figure 26 Comparison of the pressure difference

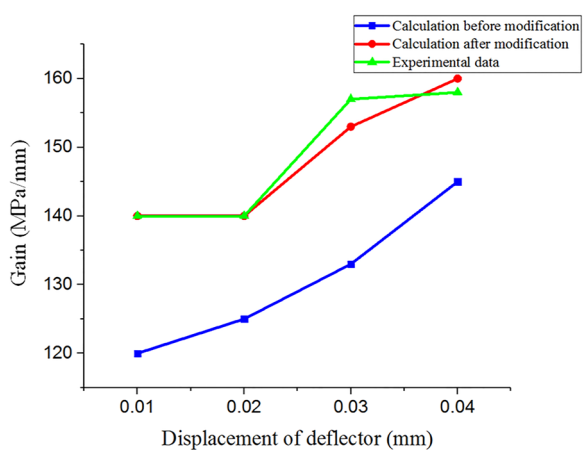

Figure 27 Comparison of the pressure gains

Figure 27. Accordingly, the modification is of great significance for modeling the servo valve.

6 Conclusions

(1) The analysis revealed that the fluid near the shunt wedge cannot resist the impact of high-speed fluid, so the assumption of the effective working length is suitable for the theoretical calculations. Because the real spatial flow in the deflector is more open, a longer core area should be given in the theoretical model.

(2) The receiver's pressure in the 3D simulation reaches 5.3 MPa, which is clearly higher than the 2D simulation result. This means that the actual energy loss from internal flow is much less than in the traditional view, because there is no significant reflux for the first jet.

(3) Different from the traditional simulated 2D flow, the 3D simulation shows that the actual flow in the deflector jet valve is a complex spatially and involves six flow phases. This discovery is favorable for understanding the complexity of the DJV's flow pattern.

Authors' Contributions

HY was in charge of the whole trial and wrote the manuscript; YR did the numerical simulation of the deflector valve's flow field; LY built the mathematical model of the deflector valve; LD plotted graphs. All authors read and approved the final manuscript.

Authors' Information

Hao Yan, born in 1979, is currently an Associate Professor at *School of Mechanical, Electronic and Control Engineering, Beijing Jiaotong University, China*. He received his PhD degree from *Harbin Institute of Technology, China*, in 2007. His research interests include mechatronics and hydraulic valves.

Yukai Ren, born in 1989, is currently a PhD candidate at *School of Mechanical, Electronic and Control Engineering, Beijing Jiaotong University, China*. He received his master degree from *North University of China, China*, in 2015. His research interests include electro-hydraulic servo valve and fluid simulation and calculation.

Lei Yao, born in 1991, is currently a master candidate at *School of Mechanical, Electronic and Control Engineering, Beijing Jiaotong University, China*. He received his bachelor degree from *Hebei Agricultural University, China*, in 2016. His research interests include electro-hydraulic servo valve.

Lijing Dong, born in 1988, is currently holding a postdoc position at *School of Mechanical, Electronic and Control Engineering, Beijing Jiaotong University, China*. She received her Ph.D. degree from the *School of Automation, Beijing Institute of Technology, China*, in 2016. Her research interests include hydraulic control systems and distributed control systems.

Competing Interests

The authors declare that they have no competing interests.

Funding

Supported by National Natural Science Foundation of China (Grant No. 51775032) and Foundation of Key Laboratory of Vehicle Advanced

Manufacturing, Measuring and Control Technology, Beijing Jiaotong University, Ministry of Education, China.

Received: 23 March 2018 Accepted: 18 March 2019
Published online: 01 April 2019

References

[1] Y C Zhu. *Fundamental research on intelligent gma for high frequency and large flow electro-hydraulic servo valve*. Tech. Rep, 2015. (in Chinese)
[2] C L Wang. *Research on key techniques of giant magnetostrictive microscale rod and film controlled fluid valve*. Tech. Rep, 2013. (in Chinese)
[3] S H Somashekhar, M Singaperumal, R K Kumar. Modelling the steady state analysis of a jet pipe electrohydraulic servo valve. *Proceedings of the Institution of Mechanical Engineers Part I Journal of Systems & Control Engineering*, 2006, 220(2): 109–129.
[4] X H S Pham. Effects of surface roughness and fluid on amplifier of jet pipe servo valve. *The International Journal of Engineering and Science (IJES)*, 2016, 5(10): 11–23.
[5] Y S Li. Mathematical modelling and characteristics of the pilot valve applied to a jet-pipe/deflector-jet servovalve. *Sensors & Actuators A Physical*, 2016, 245: 150–159.
[6] X H Wang, Z J Li, S W Sun, et al. Investigation on the prestage of a water hydraulic jet pipe servo valve based on CFD. *Applied Mechanics & Materials*, 2012, 197: 144–148.
[7] K Zhao, L D Fu, C C Zhan, et al. Flow field numerical simulation of jet pipe servo valve prestage amplifier based on fluent. *Machine Tool & Hydraulics*, 2016, 44(4): 41–43. (in Chinese)
[8] Y B Yin, Y Wang. Pressure characterization of the pre-stage of jet pipe servo valve. *Journal of Aerospace Power*, 2015, 30(12): 3058–3064. (in Chinese)
[9] K S Dhinesh. *Fluid metering using active materials*. UK: University of Bath, 2011.
[10] Y X Shang, X S Zhang, C W Hu, et al. Optimal design for amplifier of jet deflector servo valve. *Machine Tool & Hydraulics*, 2015, 43(6): 11–15. (in Chinese)
[11] H J Zhu. Simulation-modeling and fail-safe of single-stage deflector servo valve. *Hydraulics Pneumatics & Seals*, 2015, 35(11): 27–29. (in Chinese)
[12] Z G Liu, D L Yue, Z Y Yang, et al. Simulation analysis of the influence of nozzle width on the jet efficiency of deflector jet valve. *Chinese Hydraulics & Pneumatics*, 2016, (10): 27–32. (in Chinese)
[13] K Zhao. *Jet pipe servo valve flow modeling and characteristic research*. Wuhan: Wuhan University of Science and Technology, 2015. (in Chinese)
[14] Y H Yang. *Analysis and experimental research of prestage jet flow field in hydraulic servo valve*. Harbin: Harbin Institute of Technology, 2006. (in Chinese)
[15] Y B Yin, P Zhang, B Cen. Pre-stage flow field analysis on deflector jet servo valves. *Chinese Journal of Construction Machinery*, 2015, 13(1): 1–7. (in Chinese)
[16] D W Jiang, M L Xu. Simulation based on fluent for pre-stage of deflector jet servo valve. *Chinese Hydraulics & Pneumatics*, 2016(4): 48–53. (in Chinese)
[17] X H S Pham, T P Tran. Mathematical model of steady state operation in jet pipe electro-hydraulic servo valve. *Journal of Donghua University (English Edition)*, 2013, 30(4): 269–275.
[18] D K Sangiah, A R Plummer, C R Bowen, et al. A novel piezohydraulic aerospace servovalve. part 1: Design and modelling. *Proceedings of the Institution of Mechanical Engineers Part I Journal of Systems & Control Engineering*, 2013, 227(4): 371–389.
[19] C L Wang, F Ding, Q P Li, et al. Dynamic characteristics of electrohydraulic position system controlled by jet-pan servovalve. *Journal of Chongqing University*, 2003, 26(11): 11–15. (in Chinese)
[20] Y B Yin, P Zhang, Y Zhang. Analysis of the pressure characteristics of deflector jet servo valve. *Fluid Power Transmission and Control*, 2014(4): 10–15. (in Chinese)
[21] H Yan, L Bai, K Shuo, et al. Theoretical model and characteristics analysis of deflector-jet servo valves pilot stage. *Journal of Vibroengineering*, 2017, 19(6): 4655–4670.
[22] H Yan, F J Wang, C C Li, et al. Research on the jet characteristics of the deflector-jet mechanism of the servo valve. *China Phys B*, 2017, 26(4): 252–260.
[23] F J Wang, C C Li, H Yan, et al. Calculation and analysis of flow in the prestage of the deflector-jet valves. *Chinese Hydraulics & Pneumatics*, 2016(8): 74–78. (in Chinese)
[24] S J Li. *Research on mechanism of improving performance of jet servo valve by magnetic fluid*. Tech. Rep, 2006. (in Chinese)
[25] E Förthmann. Über turbulente Strahlausbreitung. *Ingenieur-Archiv*, 1934, 5(1): 42-54.
[26] C Z Yu. *Turbulent Jet*. Higher Education Press, 1993. (in Chinese)
[27] M L Albertson. Diffusion of submerged jets. *ASCE*, 1948, 115(11): 639–664.
[28] C Bourque, B G Newman. Reattachment of a two-dimensional, incompressible jet to an adjacent flat plate. *Aeronautical Quarterly*, 1960, 11(3): 201–203.